Dimers of Quadrupolar Chromophores in Solution: Electrostatic Interactions and Optical Spectra

Cristina Sissa,[†] Francesca Terenziani,[†] Anna Painelli,[†,*] Alessandro Abbotto,[‡,*] Luca Bellotto,[‡] Chiara Marinzi,[‡] Eleonora Garbin,[§] Camilla Ferrante,[§,*] and Renato Bozio[§]

Dip. Chimica GIAF, Università di Parma & INSTM UdR Parma, Parco Area delle Scienze 17/A, 43100 Parma, Italy, Dip. Scienza dei Materiali & INSTM, Università di Milano-Bicocca, via Cozzi 53, 20125 Milano, Italy, and Dip. Scienze Chimiche, Università di Padova & INSTM UdR Padova, Via Marzolo 1, 35131 Padova, Italy

Received: October 2, 2009; Revised Manuscript Received: November 26, 2009

Two dimers of a heteroaromatic quadrupolar (acceptor−donor−acceptor) chromophore have been synthesized with different interchromophoric distances. Optical spectra of dimers in solution show a red shift of the linear absorption band upon decreasing the interchromophore distance, while fluorescence and two-photon absorption spectra are only marginally affected by the interactions. A bottom up approach is adopted to describe the spectra: via a detailed spectroscopic analysis of the monomeric species in solution, we define an essential-state model for the isolated chromophore and use this information to set up a model for the dimers also accounting for interchromophore electrostatic interactions. To discriminate between static screening governed by the static dielectric constant and dynamical screening at optical frequencies, we first solve the problem in the mean-field approximation and then define the excitonic Hamiltonian on the resulting best excitonic basis. Along this line, the evolution of spectral properties with the interchromophore distance is properly rationalized.

1. Introduction

Polar and polarizable π-conjugated organic molecules have been extensively investigated in the past years for nonlinear optical (NLO) applications[1] such as electrooptic (EO) response[2] or two-photon absorption (TPA).[3] Such interest is justified by the potential use of these molecules in emerging photonic technologies, including broad-band communications and optical networking,[4] holographic memories,[5] two-photon laser scanning fluorescence microscopy,[6] optical limiting,[7] microfabrication,[8] photodynamic therapy,[9] and upconverted-lasing.[10] By far, the most successful design strategy involved π-conjugated molecules with electron donor (D) and acceptor (A) groups, and specifically, dipolar D-π-A, quadrupolar, D−π−A−π−D or A−π−D−π−A, and octupolar, D$(-\pi-A)_3$ or A$(-\pi-D)_3$, structures. On the basis of these concepts and with the guidance of relevant structure/property relationships,[11,12] several efficient dyes for NLO applications have been prepared in the past decade.[10,13–16]

In this context, some of us have designed, synthesized, and characterized a number of heteroaromatic-based dipolar dyes for EO,[17] and dipolar,[10] quadrupolar,[18] and octupolar dyes[19] for TPA. The design strategy was based on the efficient donor and accepting properties of π-excessive and π-deficient simple heteroaromatic rings.[20,21] 2,5-Bis[1-(4-*N*-methylpyridinium)ethen-2-yl)]-*N*-methylpyrrole ditriflate, **M** in Chart 1, is the most representative example of quadrupolar heteroaromatic dyes for TPA. This chromophore, with the pyrrole and the pyridinium rings acting as highly efficient D and A moieties, respectively, has a large TPA cross section[18] and found interesting applications in cellular imaging.[22]

CHART 1: Structure of the Model Chromophore and of the Dimers

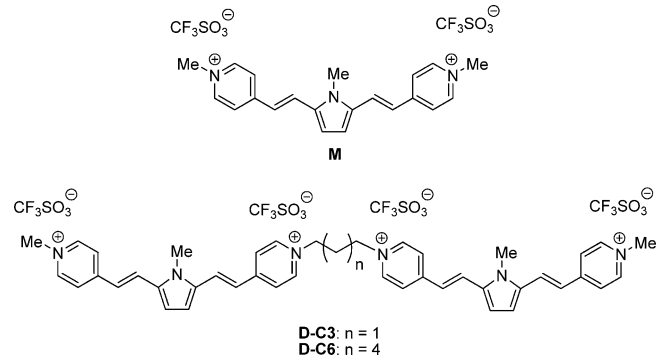

The vast majority of published studies on NLOphores is based on investigations in solution. The solvatochromism of polar (DA) chromophores has been known since 1994,[23] and the subtle effects of solvent polarity on linear and nonlinear spectra of DA chromophores have been investigated experimentally and modeled at different levels.[24,25] The anomalous solvatochromism observed in fluorescence spectra of quadrupolar and octupolar dyes has been recently explained in terms of solvent-induced symmetry breaking in the relaxed excited state.[26,27] More generally, dyes for NLO applications are largely polarizable and strongly respond to the charge distribution in the local environment.[28] Electrostatic intermolecular interactions are therefore expected to play a major role[28–30] in systems like molecular crystals,[31] films,[32] aggregates, or multichromophoric assemblies.[33,34] Possibly, one of the most impressive consequences of interchromophore interactions in clusters of dipolar dyes is the

* Corresponding author. E-mail: anna.painelli@unipr.it; alessandro.abbotto@unimib.it; camilla.ferrante@unipd.it.
† Università di Parma & INSTM UdR Parma.
‡ Università di Milano-Bicocca.
§ Università di Padova & INSTM UdR Padova.

10.1021/jp909475d
Published on Web 12/23/2009

occurrence of bistability in crystals of polar chromophores that, predicted in 2003,[29] was recently experimentally confirmed.[31]

If properly understood, interchromophore interactions offer a powerful tool to design new materials for NLO applications.[28–30] Of interest in this respect is the work done on properly engineered molecules where two or more chromophores are held together by chemical bonds: linear and nonlinear optical spectra of such multichromophoric assemblies confirmed the importance of electrostatic interactions in optical spectra.[33,34] Essential-state models for the chromophoric units[25–27] offer a general and comparatively simple scheme to describe linear and nonlinear optical properties of multichromophores, accounting for electrostatic interactions as well as for molecular vibrations and polar solvation. Modeling electrostatic interchromophore interactions while accounting for the screening from polar solvents is, however, a delicate issue.[33a,34] In the simplest approximation, two different regimes can be considered for screening. The first one corresponds to a static (or quasi static) regime: in this regime the dynamics of screened charges is much slower than all relevant degrees of freedom of the solvent, so that the screening factor is properly described by the static dielectric constant of the solvent. The second regime applies to charges with a characteristic dynamics faster than the slow (orientational, vibrational) degrees of freedom of the solvent, but slower than the fast (electronic) degrees of freedom of the solvent. In this regime, typically corresponding to optical frequencies, interactions are screened by the squared refractive index (usually measured at the sodium D line). The difference between the two screening factors is minor in nonpolar or mildly polar solvents (see as an example data in Table 1) but is very large in polar solvents ($\varepsilon/n^2 \approx 22$ for DMSO). It is therefore important to devise methods that distinguish between static interactions, like, e.g., those that determine the ground-state charge distribution in the chromophore, and dynamic interactions, like the interactions between transition dipole moments.

So far, studies on interacting chromophores for NLO have been limited to dipolar dyes. No systematic studies on discrete multichromophoric assemblies of quadrupolar dyes and on their TPA properties have been reported in the literature. This represents a strong limitation in the present investigation on TPA (multi)chromophores if one considers that quadrupolar systems are generally much more efficient two-photon absorbers than corresponding D−π−A dyes. On the basis of these premises, we present a detailed experimental and theoretical analysis of linear and nonlinear (TPA) optical properties of bichromophoric assemblies of quadrupolar dyes. To such an aim, two dimers of **M** have been synthesized where the two **M** units are joint by saturated hydrocarbon chains of different length (saturated alkyl chains having three and six carbon atoms, for **D-C3** and **D-C6**, respectively; see Chart 1). The absence of π bonds in the linking chain ensures the lack of conjugation between the two units, whereas the different length is included to control interchromophore distances. **M** bears two positive charges, and electrostatic interactions are expected to be important even in the ground state. Moreover, the two molecular arms of each **M** unit become nonequivalent in the dimer, and such symmetry lowering may induce relevant spectroscopic consequences. A proper description of the screening from the solvent becomes crucial under these conditions.

Our discussion starts with the spectroscopic analysis of **M**, whose linear absorption, fluorescence, and TPA spectra were collected in solution: a detailed analysis of these data allows the definition of a reliable essential-state model for the **M**-unit, which properly accounts for the role of molecular vibrations and polar solvation. This model sets the basis to describe interacting chromophores in the dimeric structures. Solution spectra of **D-C3** and **D-C6** dimers show an intriguing behavior: the red shift of the absorption band upon dimerization evidence sizable interchromophore interactions, while fluorescence and TPA spectra are basically unaffected by dimerization. To rationalize such behavior, on the basis of the model developed for **M**, we describe the dimer accounting for interchromophore interactions and for the coupling with slow degrees of freedom. The model is first solved in the mean-field approximation for the ground state: only static charges enter in this approximation, so that, at this stage, all interactions are screened by the static dielectric constant. The diagonalization of the mean-field problem quite naturally leads to the definition of the excitonic basis: residual electrostatic interactions in this basis describe interactions between charge distributions oscillating at optical frequencies and are screened by the squared refractive index. Along these lines we rationalize linear and nonlinear absorption spectra. The calculation of fluorescence spectra is more delicate, due to relaxation of the molecular geometry in the excited state. A mean-field approximation to the first excited state suggests the localization of the excited state and quite naturally explains the insensitivity of fluorescence spectra to interchromophore interactions.

SCHEME 1: Synthesis of the dimers D-C3 and D-C6

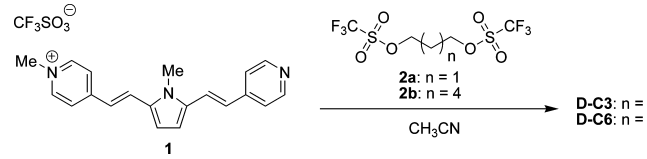

2. Experimental Section

2.1. Chromophores: General Information. NMR spectra were recorded on a Bruker AMX-500 instrument operating at 500.13 (^{1}H) and 125.77 MHz (^{13}C). Coupling constants are given in hertz. High resolution mass spectra (HRMS) were recorded using a Bruker Daltonics ICR-FTMS APEX II spectrometer equipped with an electrospray ion source (ESI). All reagents and solvents, including anhydrous solvents, were obtained from commercial suppliers and used without further purification. Reactions were monitored by thin layer chromatography using UV light (254 and 365 nm) as visualizing agent. Melting points are uncorrected. All reactions were performed in oven-dried glassware under nitrogen.

2.2. Chromophores: Synthesis. The monomer **M** was prepared according to the literature.[18] The bichromophores **D-C3** and **D-C6** were synthesized according to Scheme 1. Two equivalents of the monotriflate precursor **1**[35] were submitted to alkylation with 1 equiv of α,ω-bis(trifluoromethansulfonyl)alkane **2a**[36] or **2b**[36] in acetonitrile at room temperature, affording the expected products as dark violet solids in 70−80% yield. The quadruple saline nature (four formal positive and four formal negative charges) of the bichromophores does not make the common isolation and purification procedures (e.g., chromatography) viable. Therefore, stronger electrophiles (triflates rather than commercially available halides) needed to be synthesized for the final alkylation step, to reach high conversion yields and no presence of byproduct. Purification of the two dimers was accomplished by crystallization.

1,2-Bis{4-{{N-methyl-5-[1-(N-methylpyrid-4-yl)ethen-2-yl]pyrrol-2-yl}-ethen-2-yl}pyridinium}propane Tetratrifluoromethanesulfonate (D-C3). Trifluoromethanesulfonic anhydride (1.60 g, 954 μL, 5.67 mmol) was added dropwise to an ice cold solution

of 1,3-propanediol (0.20 g, 2.63 mmol) in anhydrous CH_2Cl_2 (20 mL), and the resulting mixture was stirred for 2 h at 0 °C. Saturated aqueous K_2CO_3 (150 mL) and CH_2Cl_2 (150 mL) were added, and the layers were separated. The aqueous layer was extracted with CH_2Cl_2 (3 × 150 mL), and the combined organic layers were dried (Na_2SO_4) and evaporated under reduced pressure, affording **2a** as a colorless oil, which was used without further purification for the next reaction (653 mg, 1.92 mmol, 73%). A solution of **1** (0.903 g, 2.00 mmol) in dry CH_3CN (45 mL) was added dropwise to a solution of ditriflate **2a** (0.34 g, 1.0 mmol) in the same solvent (35 mL), and the resulting mixture was stirred for 6 h. After cooling to 0 °C, a precipitate was obtained and collected upon filtration to afford **D-C3** as a purple solid which was submitted to recrystallization from *i*-PrOH (1.01 g, 0.81 mmol, 81%), mp >250 °C. ^{1}H NMR (DMSO-d_6): δ 8.78 (d, J = 6.4, 4 H), 8.73 (d, J = 6.4, 4 H), 8.19 (d, J = 6.4, 4 H), 8.13 (d, J = 6.4, 4 H), 8.00 (d, J = 15.8, 2 H), 7.97 (d, J = 15.8, 2 H), 7.31 (d, J = 15.7, 2 H), 7.25 (d, J = 15.8, 2 H), 7.13 (d, J = 4.4, 2 H), 7.10 (d, J = 4.4, 2 H), 4.59 (t, J = 6.8, 4 H), 4.22 (s, 6 H), 3.91 (s, 6 H), 2.65 (quintuplet, J = 6.8, 2 H). ^{13}C NMR (DMSO-d_6): δ 153.7 (C), 152.9 (C), 145.0 (CH), 144.2 (CH), 136.3 (C), 136.0 (C), 129.0 (CH), 128.4(CH), 123.5 (CH), 123.2 (CH), 121.9 (CH), 121.5 (CH), 114.2 (CH), 114.0 (CH), 57.0 (CH_2), 47.1 (CH_3), 31.4 (CH_2), 31.3 (CH_3). Anal. Calcd for $C_{47}H_{46}F_{12}N_6O_{12}S_4 \cdot 2H_2O$: C, 44.13; H, 3.94; N, 6.57. Found: C, 44.10; H, 4.03; N, 6.75.

1,2-Bis{4-{{N-methyl-5-[1-(N-methylpyrid-4-yl)ethen-2-yl]pyrrol-2-yl}ethen-2-yl}pyridinium}hexane Tetratrifluoromethanesulfonate (D-C6). Trifluoromethansulfonic anhydride (0.99 g, 590 μL, 3.5 mmol) was added dropwise to an ice cold solution of 1,6-hexanediol (450 mg, 1.60 mmol) in CH_2Cl_2 (20 mL) and the resulting mixture was stirred for 2 h at 0 °C. Saturated aqueous K_2CO_3 (100 mL) and CH_2Cl_2 (100 mL) were added, and the layers were separated. The aqueous layer was extracted with CH_2Cl_2 (3 × 100 mL), and the combined organic layers were dried and evaporated under reduced pressure affording **2b** as a colorless oil, which was used without further purification for the next reaction (500 mg, 1.36 mmol, 85%). A solution of **1** (1.26 g, 2.79 mmol) in CH_3CN (30 mL) was added dropwise to a solution of ditriflate **2b** (500 mg, 1.36 mmol) in the same solvent (25 mL), and the resulting mixture was stirred for 6 h. After cooling to 0 °C, a precipitate was obtained and collected upon filtration to afford **D-C6** as a purple solid, which was submitted to recrystallization from *i*-PrOH (1.31 g, 1.02 mmol, 75%), mp >250 °C. ^{1}H NMR (DMSO-d_6): δ 8.82 (d, J = 6.8, 4 H), 8.75 (d, J = 6.8, 4 H), 8.20 (d, J = 6.9, 4 H), 8.17 (d, J = 6.8, 4 H), 8.02 (d, J = 16.0, 2 H), 8.00 (d, J = 16.0, 2 H), 7.32 (d, J = 16.0, 2 H), 7.29 (d, J = 16.0, 2 H), 7.12 (s, 4 H), 4.45 (t, J = 7.3, 4 H), 4.21 (s, 6 H), 3.96 (s, 6 H), 1.92 (bs, 4 H), 1.35 (bs, 4 H). ^{13}C NMR (DMSO-d_6): δ 153.4 (C), 152.9 (C), 145.0 (CH), 144.1 (CH), 136.2 (C), 136.0 (C), 128.8 (CH), 128.5 (CH), 123.5 (CH), 123.2 (CH), 121.8 (CH), 121.6 (CH), 114.1 (CH), 114.0 (CH), 59.8 (CH_2), 47.1 (CH_3), 31.3 (CH_3), 30.7 (CH_2), 25.4 (CH_2). Anal. Calcd for $C_{50}H_{52}F_{12}N_6O_{12}S_4 \cdot 3H_2O$: C, 44.84; H, 4.37; N, 6.28. Found: C, 44.55; H, 4.28; N, 5.95.

2.3. Spectroscopic Measurements. Spectroscopic grade solvents were obtained by Aldrich. UV/vis spectra were collected on a Perkin-Elmer Lambda 650 spectrophotometer. Emission spectra at room temperature were recorded using a Horiba Jobin Ivon FluoroMax-3 spectrophotometer on dilute solutions (typical concentrations ~10^{-6} M). Fluorescein in NaOH 0.1 M was used as a standard (Φ = 0.9) to estimate fluorescence quantum yields. Fluorescence spectra were collected by exciting at the maximum of absorption. Fluorescence and fluorescence-excitation spectra at low temperature were measured using a liquid nitrogen cooled optical cryostat (OptistatDN, Oxford Instrument) equipped with temperature controller (ITC601, Oxford Instrument).

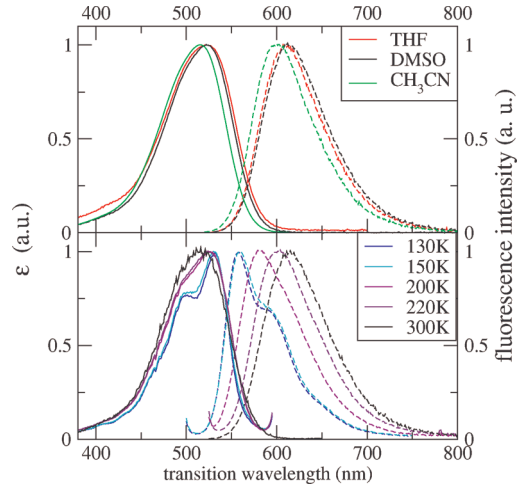

Figure 1. Top panel: absorbance (continuous lines) and fluorescence (dashed lines) spectra of **M** in three solvents of different polarity. Bottom panel: temperature evolution of absorption and fluorescence spectra of **M** in DMSO.

The TPA properties of all compounds were investigated in DMSO by the two-photon induced fluorescence (TPIF) technique.[12d] Typical concentrations for the solutions are in the range 5 × 10^{-6} to 2 × 10^{-5} M. TPIF experiments were performed using 150 fs pulses delivered from a tunable Ti:sapphire femtosecond laser system (Coherent Mira 900-F) at 76 MHz repetition rate. The TPIF excitation spectra are recorded from 740 to 930 nm with 10 nm steps. The laser beam was focused on the sample cell (a 10 mm quartz cell), via a 40 cm focal length lens. The fluorescence spectra excited by one- and two-photon excitation fell in the same spectral region, confirming that the emitting states are the same for both processes. Therefore, in the following analysis, we assume the same fluorescence quantum yield for both one- or two-photon excitation. TPA cross sections were evaluated following the procedure described in the literature[12d] and using a ~10^{-5} M solution of fluorescein in water at pH >10 (0.1 M NaOH) as a reference standard.

3. Optical Spectra of M: Essential-State Model

Due to its multisaline nature, **M** is poorly soluble in nonpolar solvents. The top panel of Figure 1 shows absorption and fluorescence spectra of **M** collected in THF (tetrahydrofuran), DMSO (dimethyl sulfoxide), and CH_3CN (acetonitrile). Figure 2 shows the TPA spectrum collected in DMSO. Table 2 summarizes experimental results for DMSO solutions. As expected for quadrupolar chromophores,[12,26] the TPA state is located at higher energies than the OPA state. The physical properties of the three solvents (dielectric constant and refractive index) are reported in Table 1: THF is a medium polarity solvent to be compared with the strongly polar DMSO and acetonitrile. We assume that the ion pairs exist as solvated free ions or solvent-separated ion pairs rather than contact ion pairs.[37] This is supported by the dissociating properties of the strongly polar DMSO and acetonitrile solvents. The similarity of optical spectra collected in THF and DMSO suggest that the same hypothesis applies in this solvent as well. Absorbance and fluorescence spectra in Figure 1a are marginally affected by the polarity of

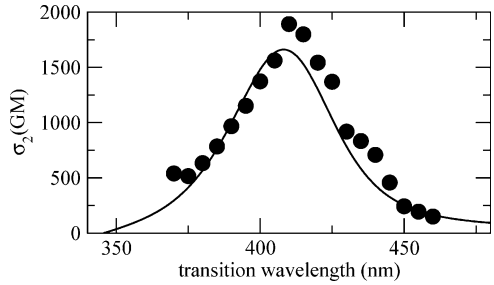

Figure 2. TPA spectrum of **M** in DMSO. Symbols show experimental data; the line represents the spectrum calculated using the model parameters in Table 3. Literature data for **M** (ref 18c) were affected by a systematic error caused by defective calibration of the fluorescence spectrometer.

TABLE 1: Dielectric Constant (ε) and Refractive Index (n) of the Solvents

solvent	ε	n
THF	7.6	1.405
CH_3CN	35.9	1.342
DMSO	46.5	1.478

TABLE 2: Spectroscopic Data for M, D-C6, and D-C3 in DMSO Solution

	λ_{abs} (nm)[a]	λ_{em} (nm)[a]	ε (cm^{-1} M^{-1})[a–c]	Φ (%)[c,d]	λ_{TPA} (nm)[a]	σ_{TPA} (GM)[a,d]
M	522	612	70 300	36	410−415	1892
D-C6	527	613	68 500	35	410−415	1857
D-C3	532	615	61 500	5.1	410−415	1807

[a] All data refer to the band maxima. [b] One- and two-photon absorption intensities are given per chromophore unit. [c] Experimental uncertainty does not exceed ±5% for ε, ± 10% for Φ, ±20% for σ_{TPA}. [d] Fluorescence quantum yield, obtained using fluorescein in NaOH 0.1 M ($\Phi = 0.9$) as a reference compound.

the solvent, suggesting that both the ground and the excited (fluorescent) states of **M** maintain a nonpolar structure: **M** is therefore classified as a class II quadrupolar dye.[26] However, when compared with spectra of typical class II quadrupolar dyes, like the squaraine dyes,[26] spectra in Figure 1a show an important Stokes-shift, suggesting that the model previously proposed for optical spectra of quadrupolar dyes[26] must be extended to account for other slow degrees of freedom in **M**. The insensitivity of the Stokes shift to the solvent polarity suggests that it is related to some internal degree of freedom not breaking the molecular symmetry. Further support to the intramolecular nature of the Stokes-shift is offered by thermochromic data in Figure 1b. The Stokes shift observed in the frozen DMSO solution at 220 K (DMSO melts at 292 K) is similar to that measured at room temperature and, in the frozen solvent, cannot be ascribed to the reorientation of solvent molecules. A sharp reduction of the Stokes shift is observed at about 150 K, where both absorption and fluorescence spectra acquire a well-developed vibronic structure. Optical spectra are only marginally affected by a further decrease of T down to 130 K. This behavior is consistent with the presence of a slow vibrational or conformational mode whose relaxation at high enough temperature is responsible for the observed Stokes shift as well as for the broadening of optical spectra. At low temperatures, this conformational mode is frozen out, resulting in a sharp reduction of both the Stokes shift and of the inhomogeneous broadening. With these considerations in mind, we propose here an essential-state model for optical spectra of **M** that represents an extension of the model originally presented in ref 26 to account for the presence of a conformational degree of freedom.

The presence of two equivalent arms in **M** immediately suggests the presence of two excited states with different symmetry. As for other multibranched chromphores,[12e] an excitonic picture of the intramolecular excitations offers a first understanding of electronic spectra. The model introduces a phenomenological interaction, J, between the two degenerate excitations in the left and right arms. As a result, the two states split into an antisymmetric and a symmetric state, whose relative energy depends on the sign of J. The two states are OPA- and TPA-active, respectively. Excitonic models were originally developed to account for intermolecular interactions in molecular aggregates and crystals.[38] In these applications, optical spectra of the isolated molecules yield information on molecular transition energies and dipole moments. Therefore, only the interaction energy J enters the model as an adjustable parameter. On the opposite, when excitonic models are applied to multibranched chromophores, the definition of excitations energies and transition dipole moments relevant to the single molecular arms is a delicate issue. As a result, most often all model parameters are freely adjustable in excitonic descriptions of multibranched chromophores.[12e] Moreover, excitonic models rely on the implicit assumption that the nature of the ground state is not affected by the interaction with the surrounding.[38] This is a poor approximation for highly polarizable and hyperpolarizable molecules like **M** and, more generally, for molecules where charge-transfer degrees of freedom play a role. In fact, in these systems the weight of charge-separated states in the ground state changes with the polarity of the local molecular environment, heavily affecting the nature of the ground as well as of the local excited states. As a consequence, different excitonic models should be defined for the same molecule in different environments, leading to a proliferation of model parameters. To overcome these difficulties and to develop a sound understanding of environmental effects on molecular spectra, in recent years some of us have developed a different strategy to describe optical spectra of dipolar and multipolar chromophores.[25–27] The approach is rooted in the well-known Mulliken model for charge-transfer excitations in molecular complexes.[39] The idea is simple and general: the low-energy states of dipolar and multipolar chromophores are dominated by charge-transfer resonances (e.g., $DA \leftrightarrow D^+A^-$ in dipolar dyes, $D^+A^-D \leftrightarrow DAD \leftrightarrow DA^-D^+$ in quadrupolar dyes, etc.). The relevant resonance structures are then chosen as basis states in the description of the system, so that the ground and excited states are expressed as linear combinations of the charge-resonating states. The nature of the ground and excited states, i.e., the weight of the resonating structures, is not fixed from the outset and, for each molecule, it readjusts in response to the local environment. The resulting families of models proved extremely powerful and were successfully applied to understand linear and nonlinear optical spectra of dipolar and multibranched chromophores in different environments.[25–34]

M is a doubly charged quadrupolar dye, whose low-energy physics can be understood accounting for the resonance between the three limiting structures: $AD^+A^+ \leftrightarrow A^+DA^+ \leftrightarrow A^+D^+A$. In the spirit of essential state models, we represent these main resonating structures in terms of three states that define the minimal basis set to describe the electronic structure of **M**. The symmetrical A^+DA^+ state, φ_0, is the lowest-energy state and plays the same role as the so-called $|N\rangle$ state in neutral quadrupolar dyes (see ref 26). Two degenerate states, φ_c and φ_s (the rationale for the c and s lettering will be clear in the next section), correspond to AD^+A^+ and A^+D^+A, respectively, and represent states where an electron is transferred from the

central donor toward one of the two lateral acceptor groups. Accordingly, a matrix element $-2^{1/2}t$ mixes φ_0 with either φ_c or φ_s to account for the finite probability of electron hopping along each molecular arm. The two degenerate states, φ_c and φ_s, play the same role as $|Z1\rangle$ and $|Z2\rangle$ in ref 26 and are separated from φ_0 by an energy gap 2η. The electronic Hamiltonian reads

$$H_{el} = -\sqrt{2}t(\hat{\sigma}_c + \hat{\sigma}_s) + 2\eta(\hat{\rho}_c + \hat{\rho}_s) \quad (1)$$

where

$$\begin{aligned} \hat{\rho}_c &= |AD^+A^+\rangle\langle AD^+A^+| \\ \hat{\rho}_s &= |A^+D^+A\rangle\langle A^+D^+A| \\ \hat{\sigma}_c &= |A^+DA^+\rangle\langle AD^+A^+| + |AD^+A^+\rangle\langle A^+DA^+| \\ \hat{\sigma}_s &= |A^+DA^+\rangle\langle A^+D^+A| + |A^+D^+A\rangle\langle A^+DA^+| \end{aligned} \quad (2)$$

In principle, the dipole moment of charged species is ill defined; however, we take advantage of the symmetric nature of **M** and describe its charge distribution in terms of a monopole and a dipole located in the molecular center. Because the monopole is invariant in all basis states, it becomes irrelevant in the discussion of solvation. On the opposite, the dipole moment vanishes in state φ_0, while φ_c and φ_s have equal and opposite dipole moments of magnitude μ_0. This dipole moment refers to states where an electronic charge is displaced along one of the molecular arms: μ_0 is therefore very large and, following Mulliken,[39] we neglect all other matrix elements of the dipole moment operator on the chosen basis. Under this approximation the dipole moment operator reads: $\hat{\mu} = \mu_0(\hat{\rho}_c - \hat{\rho}_s)$.

When an electron is transferred from the central donor toward one of the two acceptors, the relevant molecular arm relaxes: to account for this relaxation we introduce two effective molecular vibrations, q_c and q_s, with the same frequency, ω_v, and relaxation energy, ε_v.[26] Polar solvation enters the model with a reaction field, F_R, which measures the electric field generated at the solute location by the reorientation of polar solvent molecules. F_R describes a very slow motion and can be treated as a classical adiabatic coordinate. The relevant relaxation energy, ε_{or}, increases with the solvent polarity.[25] The electronic component of the reaction field, related to the deformation of the electronic charge distribution in solvent molecules surrounding the solute, corresponds instead to a fast motion with respect to the relevant degrees of freedom of the solute. It therefore enters the model with a renormalization of model parameters that, in the simplest approximation, acquire a dependence on the solvent refractive index.[25]

The Hamiltonian describing the three electronic states coupled to the two molecular coordinates and to the reaction field was derived in ref 26. However, the large and solvent-independent Stokes shift observed at room temperature cannot be reproduced unless an additional slow degree of freedom is introduced. The insensitivity of the observed Stokes shift on the solvent polarity suggests that the relevant mode corresponds to a molecular deformation. Therefore, we introduce an effective conformational coordinate, Q, with frequency ω_Q and relaxation energy ε_Q. The total Hamiltonian reads

$$\begin{aligned} H = H_{el} - \omega_v\sqrt{2\varepsilon_v}q_c\hat{\rho}_c - \omega_v\sqrt{2\varepsilon_v}q_s\hat{\rho}_s - \omega_Q\sqrt{2\varepsilon_Q}Q(\hat{\rho}_c + \hat{\rho}_s) - \\ \mu_0F_R(\hat{\rho}_c - \hat{\rho}_s) + \frac{1}{2}(\omega_v{}^2q_c{}^2 + p_c{}^2) + \frac{1}{2}(\omega_v{}^2q_s{}^2 + p_s{}^2) \\ + \frac{1}{2}\omega_Q{}^2Q^2 + \frac{\mu_0{}^2}{4\varepsilon_{or}}F_R{}^2 \end{aligned} \quad (3)$$

where H_{el} is the electronic Hamiltonian in eq 1, the second and third terms describe the linear coupling of electrons to molecular vibrations, and the fourth and fifth terms describe the coupling to the conformational coordinate and to the polar reaction field. The last four terms describe the harmonic oscillators associated with the four slow degrees of freedom: we explicitly account for the kinetic energy associated with molecular vibrations (p_c and p_s are the conjugated momenta to q_c and q_s, respectively), while the conformational coordinate Q and the solvation reaction field, F_R, are treated in the adiabatic approximation, and the relevant kinetic energy is disregarded. We assume that the two vibrational frequencies ω_v and ω_Q entering the Hamiltonian do not change with the basis state, so that the two basis states are assigned two harmonic potential energy surfaces with equal curvature but displaced minima. In other terms, we account for linear electron-vibration coupling, neglecting higher order, and quadratic terms. Assigning different frequencies to the two basis states would not alter the main physics of the system[25c-e] and would have negligible spectroscopic effects, particularly in view of the lack of resolved vibronic structure in experimental spectra.

In the isolated **M** unit the two molecular arms are equivalent and it is convenient to define symmetrized basis states, $|Z_\pm\rangle = (\varphi_c \pm \varphi_s)/2^{1/2}$, and vibrational coordinates: $q_\pm = (q_c \pm q_s)/2^{1/2}$. Only the symmetrical $|Z_+\rangle$ state is mixed to φ_0, while $|Z_-\rangle$ stays unmixed. On this basis, the electronic Hamiltonian, dependent on slow coordinates, reads

$$H_{el}^{(M)}(q_+,q_-,\tilde{Q},F_R) = \begin{pmatrix} 0 & 2t & 0 \\ 2t & 2\eta - \omega_v\sqrt{\varepsilon_v}q_+ - \sqrt{\varepsilon_Q}\tilde{Q} & -\omega_v\sqrt{\varepsilon_v}q_- - \mu_0F_R \\ 0 & -\omega_v\sqrt{\varepsilon_v}q_- - \mu_0F_R & 2\eta - \omega_v\sqrt{\varepsilon_v}q_+ - \sqrt{\varepsilon_Q}\tilde{Q} \end{pmatrix} \quad (4)$$

where the renormalized coordinate, $\tilde{Q} = \omega_Q Q$, is introduced to eliminate any explicit reference to the conformational frequency, ω_Q, that becomes irrelevant in the adiabatic approximation.

Both F_R and $\tilde{Q}$ are treated as classical coordinates, while q_+ and q_- are treated exactly, i.e., via a numerical diagonalization of the nonadiabatic Hamiltonian. Specifically, eq 1 defines, for fixed $\tilde{Q}$ and F_R values, a Hamiltonian that describes the electrons coupled to molecular vibrations. The relevant Hamiltonian matrix can be written and numerically diagonalized on a basis obtained as the direct product of the three electronic basis states (φ_0, $|Z_+\rangle$, and $|Z_-\rangle$) times the eigenstates of the two harmonic oscillators described by the sixth and seventh terms in the right-hand side of eq 1.[26] The infinite vibrational basis is truncated to include a finite number of vibrational states for each oscillator, leading to a basis of dimension $3N^2$, where N is the number of phonon states included in the basis for each oscillator. Results reported here were typically obtained setting $N = 7$. The results are not affected upon a further increase of N. Linear absorption and fluorescence spectra and two-photon absorption spectra are calculated from the resulting eigenvectors as described in detail in ref 26. The calculation is repeated for different $\tilde{Q}$ and F_R values. Resulting spectra are summed up by weighting each

TABLE 3: Essential-State Model Parameters for M

η	0.95 eV
$2^{1/2}t$	0.87 eV
ω_v	0.12 eV
ε_v	0.15 eV
ε_Q	0.25 eV
μ_0	22 D
Γ	0.1 eV
ε_{or}	THF 0.1 eV DMSO 0.25 eV

spectrum on the basis of the Boltzmann population: the ground-state energy is used to calculate populations relevant to absorption spectra, whereas fluorescence spectra are weighted on the basis of the Boltzmann population relevant to the fluorescent state.[26]

Table 3 lists the model parameters for **M**, chosen to reproduce absorption and fluorescence spectra in THF and DMSO and its TPA spectra in DMSO. Calculated spectra depend in a highly nonlinear way on the model parameters, and the optimization procedure goes via trial and error. The vibrational frequency, ω_v, and the intrinsic line width, Γ (see ref 26), have minor spectroscopic effects in view of the unresolved vibronic structure of experimental bands. Therefore, they have been fixed to reasonable values by comparison with similar systems. μ_0 only affects the intensity of the absorption spectra, while the shape and the position of absorption and fluorescence spectra show a complex interdependence on the two electronic parameters, $2^{1/2}t$ and η, and on the relaxation energies, ε_v and ε_Q. The solvent polarity plays a minor spectroscopic role in **M**, resulting in large uncertainties in the ε_{or} estimates. Calculated linear spectra are shown in Figure 3, to be compared with experimental data in the top panel of Figure 1. Calculated TPA spectra are compared with experimental data in Figure 2. We stress that all molecular parameters, including the intrinsic line width, are kept fixed in the simulations, *independent* of the solvent: only the solvent relaxation energy is tuned to account for the solvent polarity.

Both absorption and fluorescence spectra collected in CH_3CN are slightly blue-shifted with respect to spectra measured in DMSO, in spite of the similar dielectric constant of the two solvents. This anomalous behavior can be ascribed to the different refractive index of the two solvents: the smaller refractive index of CH_3CN suggests a lower stabilization of ionic states with respect to the other solvent and hence an increased η value.[25] Indeed, spectra collected in acetonitrile are very well reproduced using the same model parameters adopted for DMSO (including ε_{or}), but a slightly larger $\eta = 0.99$ eV (cf. Figure 3). We did not attempt a detailed analysis of the temperature dependence of spectra collected in DMSO in Figure 1b. In fact, both the solvent dielectric constant and refractive index depend on temperature so that not only the solvent relaxation energy (ε_{or}) but also η should be adjusted at each temperature, leading to an excessive proliferation of model parameters.

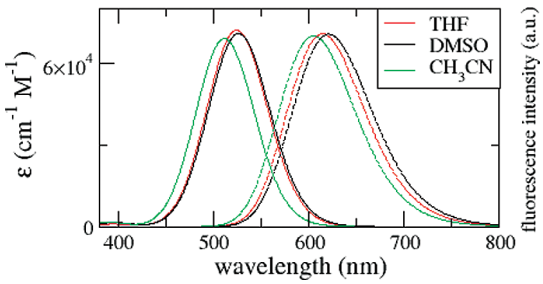

Figure 3. Calculated absorption and fluorescence spectra (continuous and dashed lines, respectively) of **M** using the model parameters listed in Table 3 (THF and DMSO). For CH_3CN we adopt the same model parameters as for DMSO with the exception of $\eta = 0.99$ eV.

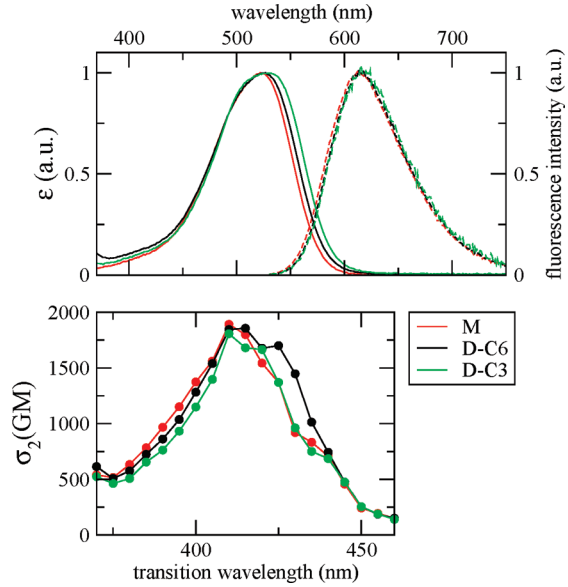

Figure 4. Optical spectra of solutions of **M**, **D-C6**, and **D-C3** in DMSO. Top panel: absorption and fluorescence spectra are shown as continuous and dashed lines, respectively; all spectra are normalized to 1. Bottom panel: dots report TPA spectra; lines are drawn as guides to the eyes. The *x*-axis is the wavelength of the transition, half the wavelength of the absorbed photon. The *y*-axis is the TPA cross section in GM: all data refer to normalized concentrations per monomeric unit.

4. Optical Spectra of Dimers: Modeling Interchromophore Electrostatic Interactions in Solution

As expected due to the presence of multiple charges (four ion pairs per molecule) the solubility of **D-C6** and **D-C3** dimers is rather poor in common organic solvents. Absorption and fluorescence spectra were successfully collected only in the strongly polar solvent DMSO. The top panel of Figure 4 shows experimental absorption and fluorescence spectra of **M**, **D-C6**, and **D-C3** in DMSO, while the bottom panel shows the corresponding TPA spectra. Fluorescence and TPA spectra of the dimeric species do not show any significant deviation from monomer spectra, whereas OPA spectra are red-shifted on going from **M** to **D-C6** and **D-C3** as a result of increasing interchromophore interactions. Understanding this behavior requires a detailed modeling of electrostatic interchromophore interactions, also accounting for screening from the surrounding solvent. DMSO is a polar solvent whose large dielectric constant almost completely suppresses static electrostatic interactions. However, excitonic interactions are screened by the squared refractive index of the solvent, with an effect more than 20 times smaller in DMSO than that due to the dielectric constant, and possibly leading to non-negligible spectroscopic effects. To distinguish between static and optical screening, we adopt a step-by-step approach: first we derive a mean-field Hamiltonian for the dimeric species that, describing the ground-state properties, accounts for static screening. Extending a procedure originally developed and exploited for clusters of dipolar (DA) chromophores,[34a,b] we then define the excitonic Hamiltonian. In this procedure, the distinction between static and optical screening emerges quite naturally leading to a proper understanding of experimental data.

TABLE 4: Basis Set for the Dimeric Structures

wave functions		charge distribution	energy	rescaled energy[a]
Φ_1	$\varphi_0\varphi_0$	$A^+DA^-A^+DA^+$	V_1	0
Φ_2	$\varphi_0\varphi_c$	$A^+DA^-AD^+A^+$	$2\eta + V_2$	$2\eta + v_2$
Φ_3	$\varphi_c\varphi_0$	$A^+D^+A-A^+DA^+$	$2\eta + V_2$	$2\eta + v_2$
Φ_4	$\varphi_0\varphi_s$	$A^+DA^+-A^+D^+A$	$2\eta + V_3$	$2\eta + v_3$
Φ_5	$\varphi_s\varphi_0$	$AD^+A^+-A^+DA^+$	$2\eta + V_3$	$2\eta + v_3$
Φ_6	$\varphi_c\varphi_c$	$A^+D^+A-AD^+A^+$	$4\eta + V_4$	$2\eta + v_4$
Φ_7	$\varphi_c\varphi_s$	$A^+D^+A-A^+D^+A$	$4\eta + V_5$	$2\eta + v_5$
Φ_8	$\varphi_s\varphi_c$	$AD^+A^+-AD^+A^+$	$4\eta + V_5$	$2\eta + v_5$
Φ_9	$\varphi_s\varphi_s$	$AD^+A^+-A^+D^+A$	$4\eta + V_6$	$2\eta + v_6$

[a] $v_i = V_i - V_1$.

4.1. Ground-State Properties: Mean-Field Approximation. In **D-C6** and **D-C3**, two **M** species are joined by a (flexible) chain through one of the two terminal A sites to define an ADA−ADA dimeric unit (Scheme 1). Accounting for three resonating structures for each chromophore, yields to nine basis states for the dimers (Table 4). The two states AD^+A^+ and A^+D^+A of each one of the two chromophores, equivalent for the isolated **M** species, become nonequivalent in the dimer. For each **M** unit in the dimer we then define the two states AD^+A^+ and A^+D^+A as φ_c or φ_s (cf Table 4) depending on the *central* (c) or *side* (s) position in each chromophore of the neutral A moiety (the A site in one **M**-unit is *central* when linked to the other chromophore, whereas it is defined as *side* when it is referred to the other A site). Electrostatic interchromophore interactions affect the energy of the basis states, as shown in the last two columns of Table 4. Specifically, the V_i energies (or the rescaled energies $v_i = V_i - V_1$) describe the electrostatic interactions between the different charge distributions and can therefore be calculated from the mutual arrangement of the monomers once a specific model is adopted for the charge distribution.[28–30] As schematically shown in Figure 5, we represent each chromophore as a rigid rod of total length $2l$ (l is the effective length of a D−A subunit), where two positive point charges are located, depending on the state, either at the two A groups at the extreme sites of the rod and/or at the D group in the middle. The two chromophores are joined through the A sites by a link of length r. Finally, different geometries are defined by varying the angle φ from 0, accounting for two faced **M** units, up to 180°, corresponding to two aligned **M** units pointing in opposite directions (Figure 5, right panel). As shown in Figure 5, we have constrained the two chromophores in perpendicular planes with respect to the joining link: the resulting geometries, however, span a wide enough subset of geometries to reliably understand spectroscopic effects of interchromophore interactions. On the basis of these premises, the V_i interactions shown in Table 4 are calculated by summing up interchromophore interactions between point charges. For fixed l, the V_i interactions depend on r and φ, and being interested in ground-state (i.e., static) properties, they are screened by the static dielectric constant (explicit expressions for V_i energies are given in the Supporting Information).

First, we focus our attention on the electronic problem. The relevant Hamiltonian is the sum of the two electronic Hamiltonians for each unit (eq 1) and of a term that describes electrostatic interchromophore interactions:

$$H_{el} = -\sqrt{2}t\sum_i(\hat{o}_c^i + \hat{o}_s^i) + (2\eta + v_2)\sum_i \hat{\rho}_c^i + (2\eta + v_3)\sum_i \hat{\rho}_s^i + (v_4 - 2v_2 - 2v_3)\hat{\rho}_c^1\hat{\rho}_c^2 + (v_6 - 2v_2 - 2v_3)\hat{\rho}_s^1\hat{\rho}_s^2 + (v_5 - v_2 - v_3)(\hat{\rho}_c^1\hat{\rho}_s^2 + \hat{\rho}_s^1\hat{\rho}_c^2) \quad (5)$$

where the $i = 1, 2$ apex on the $\hat{o}$ and $\hat{\rho}$ operators (cf. eq 3) runs on the two chromophoric units. In the ground state the two molecules are equivalent so that just two order parameters are required, $\rho_c = \langle\hat{\rho}_c^1\rangle = \langle\hat{\rho}_c^2\rangle$ and $\rho_s = \langle\hat{\rho}_s^1\rangle = \langle\hat{\rho}_s^2\rangle$, where $\langle\ \rangle$ indicates the ground-state expectation value. We define the deviation operators as $\hat{\delta}_{c/s}^i = \hat{\rho}_{c/s}^i - \langle\hat{\rho}_{c/s}^i\rangle$: the mean-field approximation neglects in the above Hamiltonian all nonlinear terms in the deviation operators. In this approximation, the problem reduces to the diagonalization of the Hamiltonian for an isolated chromophore subject to the electrostatic potential generated by the (frozen) charge distribution on the nearby chromophore:

$$H_{el}^{mf} = -\sqrt{2}t(\hat{o}_c^i + \hat{o}_s^i) + 2\eta_c\hat{\rho}_c^i + 2\eta_s\hat{\rho}_s^i \quad (6)$$

The mean-field Hamiltonian coincides in fact with the Hamiltonian of the isolated **M** molecule (cf. eq 1), but the η energy is substituted by effective $\eta_{c/s}$ energies that account for the interaction of each chromophore with the average charge distribution on the nearby chromophore. The two arms of each **M** unit are not equivalent in the dimer and two different η values are associated with the φ_c and φ_s states, as follows:

$$2\eta_c = 2\eta + v_2 + (v_4 - 2v_2 - 2v_3)\rho_c + (v_5 - v_2 - v_3)\rho_s$$
$$2\eta_s = 2\eta + v_3 + (v_6 - 2v_2 - 2v_3)\rho_s + (v_5 - v_2 - v_3)\rho_c \quad (7)$$

These equations show that the energies of the φ_c and φ_s states of each **M** unit self-consistently depend on the charge distribution on the nearby molecule, as described by the two order parameters ρ_c and ρ_s. The mean-field Hamiltonian matrix is easily written and diagonalized on the basis of the three states, φ_0, φ_c, and φ_s. We impose self-consistency with the requirement that the $\rho_{c/s}$ values entering the mean-field Hamiltonian matrix coincide with the squared coefficients of the $\varphi_{c/s}$ in the ground-state wave function. Specifically, we start with a guess for $\rho_{c/s}$, diagonalize the resulting mean-field Hamiltonian, calculate new estimates of $\rho_{c/s}$ as the squared coefficient of the $\varphi_{c/s}$ functions, and repeat the procedure until successive $\rho_{c/s}$ values differ less than a predefined precision (typically set to 10^{-8}).

Each chromophoric unit in the dimer is described in terms of the same model derived for the isolated **M** unit in the previous section. Therefore, we introduce two vibrational coordinates

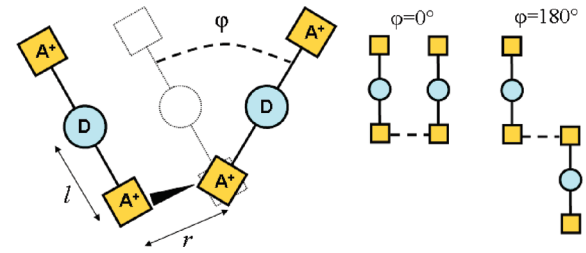

Figure 5. Left panel: schematic view of the dimer geometry, with the definition of geometrical parameters. Right panel: top view of two special cases $\varphi = 0$ and $\varphi = 180°$.

$q^i_{c/s}$ ($i = 1, 2$), one conformational coordinate $\tilde{Q}^i$ and one solvent reaction field F^i_R for each chromophore. These slow coordinates are coupled to the charge distribution in each chromophore as described in eq 3. We work in the adiabatic approximation and use the Hellman−Feynman theorem to minimize the ground-state energy and find the equilibrium positions for the slow coordinates as follows (cf. eq 3):

$$\begin{aligned}(q^i_{c/s})_{eq} &= \frac{\sqrt{2\varepsilon_v}}{\omega_v}\rho_{c/s}\\ (\tilde{Q}^i)_{eq} &= \sqrt{2\varepsilon_Q}(\rho_c + \rho_s)\\ (F^i_R)_{eq} &= \frac{2\varepsilon_{or}}{\mu_0}(\rho_c - \rho_s)\end{aligned} \tag{8}$$

Inserting these equilibrium coordinates into the coupling Hamiltonian in eq 3, we end up with a complete mean-field Hamiltonian that accounts in an averaged form for the mutual interaction between the two chromophores and for the coupling to slow (vibrational, conformational, and environmental) degrees of freedom. This Hamiltonian has again the form in eq 6, but with renormalized $\eta_{c/s}$ parameters:

$$\begin{aligned}2\eta_c = 2\eta + v_2 + (v_4 - 2v_2 - 2v_3)\rho_c + (v_5 - v_2 - v_3)\rho_s\\ - 2\varepsilon_v\rho_c - 2\varepsilon_Q(\rho_c + \rho_s) - 2\varepsilon_{or}(\rho_c - \rho_s)\\ 2\eta_s = 2\eta + v_3 + (v_6 - 2v_2 - 2v_3)\rho_s\\ + (v_5 - v_2 - v_3)\quad \rho_c - 2\varepsilon_v\rho_s - 2\varepsilon_Q(\rho_c + \rho_s) - 2\varepsilon_{or}(\rho_c - \rho_s)\end{aligned} \tag{9}$$

The complete mean-field Hamiltonian is finally diagonalized, following the same self-consistent procedure described above, to get the ground state, g, and the two excited states, c and e, with excitation energies E_c and E_e, respectively.

The large screening of electrostatic interactions in DMSO results in minor effects of interchromophore interactions in the ground-state properties of dimeric species. In particular, as discussed above, each chromophore in the dimer has a lower symmetry than the isolated **M** unit, but the effects of this symmetry lowering are very weak. In particular, Figure 6 shows the evolution of $\rho_c - \rho_s$ as a function of the intermolecular distance and of the torsion angle (cf. Figure 5) calculated in the mean-field approximation for a **D** unit in DMSO. We adopt for the **M** subunits the same model parameters as obtained in the previous section (Table 2) and calculate the electrostatic interchromophore interactions, v_i, setting $l = 8$ Å, and accounting for the screening due to the static dielectric constant of DMSO (Table 1, cf. Supporting Information). When the two molecules are faced ($\varphi = 0$), the symmetry of the isolated **M** unit is maintained, irrespective of the interchromophore distance,

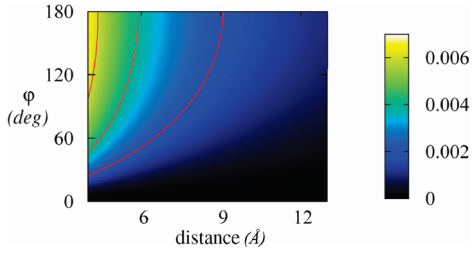

Figure 6. Mean-field results for **D**. The color map shows $\rho_c - \rho_s$ as a function of r and φ (cf. Figure 5). Molecular parameters are taken from Table 2, and we set $l = 8$ Å.

TABLE 5: Excitonic Basis for the Dimeric Structures

wave functions		mf energies
Ψ_1	gg	0
Ψ_2	gc	E_c
Ψ_3	cg	E_c
Ψ_4	ge	E_e
Ψ_5	eg	E_e
Ψ_6	cc	$E_c + E_c$
Ψ_7	ce	$E_c + E_e$
Ψ_8	ec	$E_c + E_e$
Ψ_9	ee	$E_e + E_e$

and $\rho_c - \rho_s = 0$. Deviations from this limit are observed at small distances and large φ angles. However, on an absolute scale, $\rho_c - \rho_s$ stays small, and in fact no hint of the symmetry lowering is recognized in optical spectra of either **D-C6** or **D-C3**.

4.2. Linear and Nonlinear Absorption Spectra: Setting up the Exciton Approximation. As long as we are interested in static properties of dimeric units, relevant interchromophore interactions are screened by the static dielectric constant. However, the energies of optical excitations are strongly affected by excitonic interactions.[38] These describe electrostatic interactions between transition dipoles oscillating at optical frequencies and are therefore screened by the squared refractive index at optical frequency.[38] A strategy is required to single out excitonic interactions as to properly screen them.

A good starting point to set up the excitonic model is offered by the solution of the mean-field problem.[29,30] According to the literature,[29,30] we define the best excitonic basis functions, Ψ_i in Table 5, as the direct product of the mean-field eigenstates g, c, and e obtained by the self-consistent diagonalization of the mean-field Hamiltonian for the two **M** units. In other words, we choose the excitonic basis as the eigenstates of the dimer Hamiltonian in the mean-field approximation. Among the basis states we recognize the ground state, Ψ_1, two states with a single c excitation (Ψ_2 and Ψ_3), two states with a single e excitation (Ψ_4 and Ψ_5), and states where both molecules are excited (Ψ_{6-9}). The corresponding mean-field energies (third column in Table 5) are simply the sum of the mean-field energies relevant to the two chromophores. The g, c, and e states, obtained from the diagonalization of the monomer Hamiltonian, are expressed as linear combinations of the basis states φ_0, φ_c, and φ_s on each chromophore, so that the Ψ_i functions are linear combinations of the Φ_i functions. Then a linear transformation allows us to rewrite the dimer Hamiltonian from the Φ_i to the Ψ_i basis. If the excitonic approximation works well,[28,29,38] the off-diagonal elements of the Hamiltonian matrix written on the excitonic basis are small with respect to the excitation energies, and the nondiagonal matrix elements of the Hamiltonian matrix have negligible effects, with the notable exception of those nondiagonal elements mixing up degenerate states (i.e., Ψ_2 and Ψ_3, Ψ_4 and Ψ_5, Ψ_7 and Ψ_8, cf. Table 5).

The excitonic Hamiltonian for the dimer is then obtained by neglecting all off-diagonal elements of the Hamiltonian written on the excitonic basis, with the exception of those connecting degenerate states. Moreover, in the residual off-diagonal terms, the contributions arising from electrostatic interchromophore interactions is multiplied by a factor ε/n^2, to renormalize the excitonic interaction energies for the screening at optical frequencies. The diagonalization of the resulting excitonic Hamiltonian finally leads to the excited states calculated for all slow coordinates fixed at their equilibrium position obtained in the adiabatic approximation for the ground state. With this information we can calculate *vertical* OPA and TPA frequencies

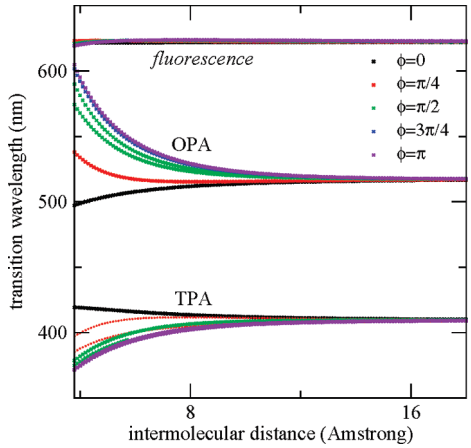

Figure 7. Transition (OPA, TPA, and fluorescence) energies calculated in the excitonic model (see text) for **D** as a function of the intermolecular distance and for different torsion angles. Molecular parameters are taken from Table 3, and $l = 8$ Å. Only the most intense transitions are shown for OPA and TPA spectra. For some φ values, due to the lowering of the molecular symmetry as due to electrostatic interactions, a splitting of the OPA and TPA transitions is observed.

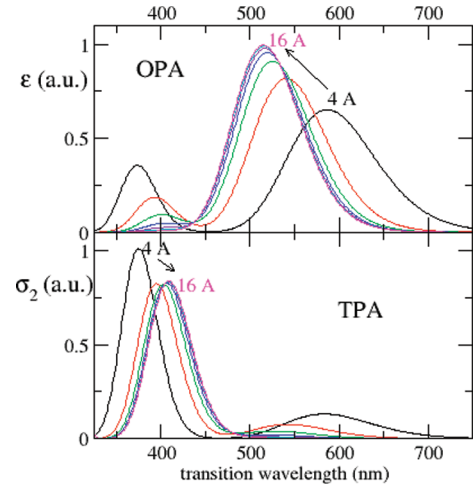

Figure 8. OPA (top) and TPA (bottom) spectra calculated for a dimeric unit with $\varphi = 135°$ and variable interchromophore distance (from 4 to 16 Å, with 2 Å steps).

and intensities. Figure 7 collects information on transition energies, calculated for a dimer **D** as a function of the interchromophore distance for different angles φ. As expected, when the intermolecular distance becomes large ($\gtrsim$12 Å) we regain the result for the **M** molecule in DMSO, irrespective of the mutual orientation of the chromophores. Sizeable and φ-dependent excitonic effects are observed upon decreasing r below ~10 Å. Quite interestingly, excitonic interactions affect both OPA and TPA frequencies, a result that points to the failure of the dipolar approximation for electrostatic interactions.[29] We notice that, for $\varphi > 0$, interchromophore interactions lower the symmetry of each **M** unit; as a result, a sizable splitting of the OPA and/or TPA bands is observed in some cases (cf. Figure 7). The splitting is, however, too small to be recognized in the broad experimental spectra.

With regard to OPA, the transition is red-shifted by interchromophore interactions for all angles apart from the special case of $\varphi = 0$ (i.e., for faced **M** units) where it is blue-shifted. This special geometry is unlikely to occur because of electrostatic repulsion (at least when interchromophore distances are small enough to give rise to sizable interaction). On this basis, data in Figure 7 nicely agree with the experimentally observed red shift of the linear absorption band upon decreasing the interchromophore distance. Of course, our model for electrostatic interactions is fairly rough, so that intermolecular distances represent effective values. However, results in Figure 7 suggest that for **D-C6**, with an approximate interchromophore distance of about 8 Å, OPA and TPA spectra are marginally affected by interchromophore interactions. On the contrary, in **D-C3** $r \approx 6$ Å and a sizable red shift (≈10−20 nm) is predicted in OPA spectra, in good agreement with experimental data. The smaller red shift expected for the TPA band is hardly recognized in experimental spectra, mainly due to the intrinsic lower resolution of TPA data (spectral resolution of TPA data is dictated by the spectral width of the Gaussian-shaped excitation pulses produced by the laser). The intensities of the OPA and TPA bands are only marginally affected up to the distances relevant for the species **D-C3**, with just a small decrease of the OPA intensity (as shown in Figure 8 for $\varphi = 135°$).

The detailed calculation of OPA and TPA spectra, including the vibronic structure and accounting for the inhomogeneous broadening from polar solvent, is extremely demanding for the dimeric unit. In fact, this would require the diagonalization of the nonadiabatic Hamiltonian for a system with 9 electronic states and 4 vibrational degrees of freedom. With the conservative estimate of 5 vibrational states for each degree of freedom, one should diagonalize (getting all eigenstates and transition dipole moments) a square matrix of dimension 5625,[2] and the calculation should be repeated by exploring the phase space spanned by 4 classical fields, leading to an overwhelmingly big number of calculations. Therefore, we limit attention to vertical transition frequencies and intensities, obtained in the excitonic approximation. To offer some information on the calculated spectral evolution, the two panels of Figure 8 describe, as a typical example, the evolution with the interchromophore distance of OPA and TPA spectra for a dimer with $\varphi = 135°$, calculated by assigning to each electronic state (as obtained from the diagonalization of the excitonic model) a Gaussian line shape with full-width at half-maximum of ≈2000 cm^{-1}.

As previously discussed,[28] when mean-field excitation energies are comparable with electrostatic interactions, the off-diagonal matrix elements neglected in the excitonic approximation may play a role. For some of these ultraexcitonic terms, like for instance those mixing the ground and excited states, it is not obvious which kind of screening, either static or optical, should be adopted. We have explicitly verified that these terms, irrespective of the adopted screening model, marginally affect calculated spectra: the excitonic approximation works well in our case.

4.3. Fluorescence Spectra: The Relaxed Excited State. Steady-state fluorescence occurs from the relaxed first excited state. Therefore, the calculation of the fluorescence spectrum requires, as a first step, a mean-field model for the relaxed fluorescent state. The problem is more delicate than the one described in section 4.1 because the first excited state of the dimeric unit corresponds to a state where only one out of the two chromophores is excited, whereas the ground state is unique. To account for the nonequivalence of the two molecular units, we have developed a mean-field model based on four order parameters, and specifically, $\rho_{c1} = \langle \hat{\rho}_c^! \rangle$, $\rho_{s1} = \langle \hat{\rho}_s^! \rangle$, for the first chromophore (chromophore 1), and the two corresponding parameters for the second chromophore (chromophore 2). In the mean-field approximation, the dimer Hamiltonian splits in two Hamiltonians, H_i^{mf}, relevant to each **M** unit. Each one of these Hamiltonians has exactly the same form as the mean field Hamiltonian in eq 6:

$$H_1^{\mathrm{mf-fluo}} = -\sqrt{2}t(\hat{\sigma}_c^1 + \hat{\sigma}_s^1) + 2\eta_{c1}\hat{\rho}_c^1 + 2\eta_{s1}\hat{\rho}_s^1$$
$$H_2^{\mathrm{mf-fluo}} = -\sqrt{2}t(\hat{\sigma}_c^2 + \hat{\sigma}_s^2) + 2\eta_{c2}\hat{\rho}_c^2 + 2\eta_{s2}\hat{\rho}_s^2 \quad (10)$$

but a different sets of η energies is now defined for each **M** unit, as follows:

$$\begin{aligned}
2\eta_{c1} &= 2\eta + v_2 + (v_4 - 2v_2 - 2v_3)\rho_{c2} + (v_5 - v_2 - v_3)\rho_{s2} \\
&\quad - 2\varepsilon_v\rho_{c1} - 2\varepsilon_Q(\rho_{c1} + \rho_{s1}) - 2\varepsilon_{or}(\rho_{c1} - \rho_{s1}) \\
2\eta_{s1} &= 2\eta + v_3 + (v_6 - 2v_2 - 2v_3)\rho_{s2} + (v_5 - v_2 - v_3)\rho_{c2} \\
&\quad - 2\varepsilon_v\rho_{c1} - 2\varepsilon_Q(\rho_{c1} + \rho_{s1}) - 2\varepsilon_{or}(\rho_{c1} - \rho_{s1}) \\
2\eta_{c2} &= 2\eta + v_2 + (v_4 - 2v_2 - 2v_3)\rho_{c1} + (v_5 - v_2 - v_3)\rho_{s1} \\
&\quad - 2\varepsilon_v\rho_{c2} - 2\varepsilon_Q(\rho_{c2} + \rho_{s2}) - 2\varepsilon_{or}(\rho_{c2} - \rho_{s2}) \\
2\eta_{s2} &= 2\eta + v_3 + (v_6 - 2v_2 - 2v_3)\rho_{s1} + (v_5 - v_2 - v_3)\rho_{c1} \\
&\quad - 2\varepsilon_v\rho_{c2} - 2\varepsilon_Q(\rho_{c2} + \rho_{s2}) - 2\varepsilon_{or}(\rho_{c2} - \rho_{s2})
\end{aligned} \quad (11)$$

The effective η energies for each chromophoric unit depend, through electrostatic interactions, on the charge distribution on the nearby chromophore, and through the coupling to slow degrees of freedom, on the charge distribution on the chromophore itself. Of course, being interested in stationary results, the electrostatic interactions in the above equations are screened by the static dielectric constant. To solve the mean-field problem, we start with a guess for the four order parameters, diagonalize the two Hamiltonians in eq 10, and recalculate the order parameters as the expectation values of the relevant operators on the *ground states* for chromophore 1 and on the *first excited state* for chromophore 2. The new estimates for the order parameters enter the mean-field Hamiltonians in eq 10, and the procedure is repeated until convergence.

Figure 9 shows results obtained along these lines: in particular, the asymmetry, $\rho_{ci} - \rho_{si}$, calculated for each chromophore ($i = 1, 2$) is shown as a function of r and φ. In the proposed approach the excitation is localized (by construction) on chromophore 2, and in fact, the results shown in the figure for chromophore 1 are similar to those calculated for the ground state (cf. Figure 6). On the opposite, chromophore 2 shows a much larger asymmetry, with $\rho_{c2} - \rho_{s2}$ ranging from 0.25 to 0.45, a result easily rationalized on the basis of the larger polarizability of the chromophore in the excited state.

Once the mean-field solution is obtained, one can proceed to the construction of the excitonic model relevant to fluorescence, along the same lines as discussed in section 4.1. In particular, the total dimer Hamiltonian is rewritten on the relevant excitonic basis, obtained as the direct product of the mean field eigenstates for the first and second chromophore. The excitonic approximation now amounts to neglect of all off-diagonal elements of the second row and column that would mix the first excited state, already optimized at the mean-field level, to the other states. All non-neglected matrix elements of the transformed matrix coming from electrostatic interactions are then renormalized by n^2/ε, to account for screening at optical frequencies. Finally, transition energies and dipole moments are obtained via a numerical diagonalization. In agreement with experimental data, the calculated fluorescence frequency is marginally affected by intermolecular interactions (Figure 7), due to the effective localization of the relaxed excited state.

5. Conclusions

Interchromophore interactions play a major role in the definition of the properties and behavior of molecular materials.[28–31,38] The effects are particularly intriguing in materials for NLO that are made up by chromophores that, by definition, respond in a large and nonlinear way to external stimuli.[28–30] If properly investigated and rationalized, interchromophore interactions may offer a powerful tool to tune the material response and design efficient and custom-tailored materials.

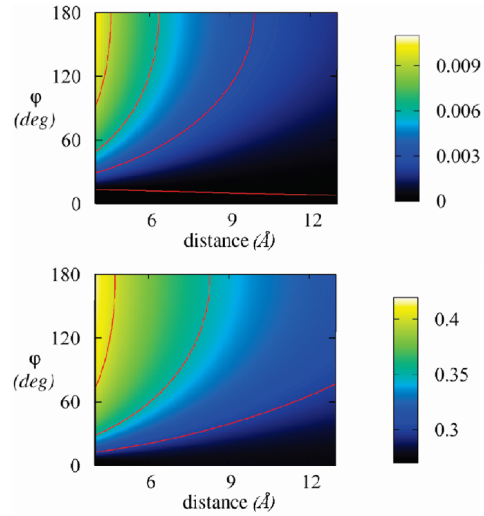

Figure 9. Mean-field results for the fluorescent state. Top and bottom panels show $\rho_c - \rho_s$ values obtained for the first and second chromophore, respectively. Molecular parameters are taken from Table 3, and $l = 8$ Å.

We have presented a multidisciplinary investigation (organic synthesis, linear and nonlinear spectroscopic investigation, theoretical modeling) on bichromophoric assemblies based on a highly efficient TPA quadrupolar (ADA) dye. The dimers were obtained by linking two quadrupolar chromophores through their terminal acceptor moieties. The use of saturated alkyl chains of different length excludes π-conjugation effects between the two units and accounts for different interchromophore distances. Linear absorption and fluorescence spectra were collected in several solvents for the monomeric unit **M**, whereas linear absorption and fluorescence spectra and TPA spectra of the two dimeric species were collected in DMSO. The linear absorption peak is red-shifted on going from **M** to **D** with a slight decrease of the molar extinction coefficient (normalized per chromophore unit). In contrast, TPA maximum wavelengths and cross sections are unaffected, within experimental uncertainties, by intermolecular interactions. The fluorescence quantum yield decreases with increasing interchromophore interactions, probably due to the opening of new relaxation channels, but the position and shape of the fluorescence band is not affected upon dimerization.

Bottom-up modeling strategies[28–30] proved very useful to investigate the role of electrostatic interchromophore interactions in materials based on polar donor−acceptor molecules.[31,32,33a,b,34] These strategies take advantage of the molecular nature of the materials of interest and start from a detailed analysis of optical spectra of isolated chromophores in solution to define reliable essential-state models for the specific chromophores. This information is then used to build models for interacting chromophores in molecular crystals, films, aggregates, and multichromophoric assemblies. When discussing electrostatic interactions in multichromophoric assemblies in solution, particular attention must be paid to screening effects from the solvent.[33a,34] Indeed, the dielectric constant of typical organic solvents spans more than 1 order of magnitude from ≈2 for nonpolar solvents up to ≈50 for strongly polar solvents. The screening of electrostatic interaction would suggest negligible effects of interchromophore interactions in strongly polar

solvents. However, it is well-known[38] that excitonic interactions involve transition charge densities and, as such, should be screened by the squared refractive index of the solvent as measured at optical frequencies: the resulting screening constant is rather small (again of the order of 2) and similar for most organic solvents. Discriminating between static and dynamic screening is a tough problem that has been addressed for interacting dipolar chromophores in solution[34a,b] exploiting the analytical transformation toward the excitonic basis.[29] The approach is based on the solution of the mean-field problem for interacting chromophores and the subsequent transformation of the Hamiltonian for interacting chromophores in the so-called excitonic basis, i.e., the eigenstates of the mean-field Hamiltonian. Adopting the same procedure for interacting quadrupolar (or multipolar) chromophores is nontrivial. First of all, interchromophore interactions in general lower the symmetry of the chromophores so that multiparameter mean-field approaches must be devised. Moreover, the analytical transformation toward the excitonic basis adopted for interacting DA chromophore does not apply to multipolar dyes and one has to resort to a numerical transformation.

All these problems have been faced and solved in this work that describes a numerical approach to treat interchromophore interactions in dimers of quadrupolar chromophores in solution. We notice that the model also accounts for the coupling to solvation and vibrational degrees of freedom in the adiabatic approximation. The proposed strategy is general and can be extended to larger clusters of multipolar chromophores as well. In the process, in line with the bottom-up modeling strategy, we have analyzed in detail optical spectra of the isolated **M** chromophore in different solvents and have defined a reliable three-state model for this interesting dye, also accounting for the coupling between electrons and slow degrees of freedom, including molecular vibrations and effective solvation coordinates. The effects of electrostatic interchromophore interactions observed in the investigated systems are rather small, mainly as a result of the fairly large interchromophore distances in both dimers. We have adopted a very simple model for electrostatic interactions, based on point charges centered on D and A sites. More refined models can be envisaged, on the basis of more realistic descriptions of the charge distribution in the chromophoric units,[31] leading to different V_i values. However, the proposed approach to account for interchromophore interactions and to discriminate between static and dynamic screening applies quite irrespective of the specific model adopted for the electrostatic interactions. In spite of using a fairly simple model for electrostatic interactions, the spectroscopic effects of interchromophore interactions are well accounted for in the proposed model. In particular, the absorption band red-shifts upon decreasing the interchromophore distance from the solvated **M** to **D-C6** and **D-C3**, while the fluorescence band is totally unaffected by the interchromophore separation. This puzzling result is well reproduced by our calculation, and the insensitivity of the fluorescence band to the interchromophore distance is safely ascribed to the localized nature of the relaxed fluorescent state.

Acknowledgment. Work supported by MIUR-PRIN 2006-031511 "Chromophores in organic and hybrid nanostructures: supramolecular engineering of photonic properties" and MIUR-FIRB RBNE033KMA.

Supporting Information Available: Explicit expressions for the electrostatic interactions energies v_i in Table 4. This material is available free of charge via the Internet at http://pubs.acs.org.

References and Notes

(1) (a) *Molecular Nonlinear Optics*; Zyss, J., Ed.; Academic Press: New York, 1994. (b) Burland, D. M. Optical Nonlinearities in Chemistry. *Chem. Rev.* **1994**, *94*, 1–278. (c) Prasad, P. N.; Williams, D. J. *Introduction to Nonlinear Optical Effects in Molecules and Polymers*; Wiley: New York, 1991.

(2) *Polymers for Second-Order Nonlinear Optics*; Lindsay, G. A.; Singer, K. D.; Eds.; ACS Symposium Series 601; American Chemical Society: Washington, DC, 1995.

(3) (a) Terenziani, F.; Katan, C.; Blanchard-Desce, M.; Badaeva, E.; Tretiak, S. *Adv. Mater.* **2008**, *20*, 4641–4678. (b) He, G. S.; Tan, L. S.; Zheng, Q.; Prasad, P. N. *Chem. Rev.* **2008**, *108*, 1245–1330. (c) Pawlicki, M.; Collins, H. A.; Denning, R. G.; Anderson, H. L. *Angew. Chem., Int. Ed.* **2009**, *48*, 3244–3266.

(4) (a) Dalton, L. R. *J. Phys.: Condens. Matter* **2003**, *15*, R897–R934. (b) Ma, H.; Jen, A. K.-Y.; Dalton, L. R. *Adv. Mater.* **2002**, *14*, 1339–1365. (c) Ermer, S.; Lovejoy, S. M.; Bedworth, P. V.; Leung, D. S.; Warren, H. B.; Epstein, J. A.; Girton, D. G.; Dries, L. S.; Taylor, R. E.; Barto, R. R. J.; Eades, W.; Van Eck, T. E.; Moss, A. S.; Anderson, W. W. *Adv. Funct. Mater.* **2002**, *12*, 605–610. (d) Lee, M.; Katz, H. E.; Erben, C.; Gill, D. M.; Gopalan, P.; Heber, J. D.; McGee, D. J. *Science* **2002**, *298*, 1401–1404. (e) Shi, Y. Q.; Zhang, C.; Zhang, H.; Bechtel, J. H.; Dalton, L. R.; Robinson, B. H.; Steier, W. H. *Science* **2000**, *288*, 119–122.

(5) Kippelen, B.; Blanche, P.-A.; Schulzgen, A.; Fuentes-Hernandez, C.; Ramos-Ortiz, G.; Wang, J.-F.; Peyghambarian, N.; Marder, S. R.; Leclercq, A.; Beljonne, D.; Brédas, J.-L. *Adv. Funct. Mater.* **2002**, *12*, 615–620.

(6) (a) Denk, W.; Strickler, J. H.; Webb, W. W. *Science* **1990**, *248*, 73–76. (b) Gura, T. *Science* **1997**, *276*, 1988–1990. (c) Cox, G. *Mater. Today* **2002**, *5*, 34–41. (d) Larson, D. R.; Zipfel, W. R.; Williams, R. M.; Clark, S. W.; Bruchez, M. P.; Wise, F. W.; Webb, W. W. *Science* **2003**, *300*, 1434–1437.

(7) (a) Signorini, R.; Pedron, D.; Ferrante, C.; Bozio, R.; Brusatin, G.; Innocenzi, P.; Della Negra, F.; Maggini, M.; Abbotto, A.; Beverina, L.; Pagani, G. *SPIE Proc.* **2003**, *4797*, 1–14. (b) Ehrlich, J. E.; Wu, X. L.; Lee, L. Y. S.; Hu, Z. Y.; Rockel, H.; Marder, S. R.; Perry, J. W. *Opt. Lett.* **1997**, *22*, 1843–1845.

(8) (a) Zhou, W.; Kuebler, S. M.; Braun, K. L.; Yu, T.; Cammack, J. K.; Ober, C. K.; Perry, J. W.; Marder, S. R. *Science* **2002**, *296*, 1106–1109. (b) Cumpston, B. H.; Ananthavel, S. P.; Barlow, S.; Dyer, D. L.; Ehrlich, J. E.; Erskine, L. L.; Heikal, A. A.; Kuebler, S. M.; Lee, I. Y. S.; McCord-Maughon, D.; Qin, J. Q.; Rockel, H.; Rumi, M.; Wu, X. L.; Marder, S. R.; Perry, J. W. *Nature* **1999**, *398*, 51–54. (c) La Fratta, C. N.; Fourkas, J. T.; Baldacchini, T.; Farrer, R. A. *Angew. Chem. Int. Ed.* **2007**, *46*, 6238–6258.

(9) (a) Konan, Y. N.; Gurny, R.; Allemann, E. *J. Photochem. Photobiol. B* **2002**, *66*, 89–106. (b) Frederiksen, P. K.; Jorgensen, M.; Ogilby, P. R. *J. Am. Chem. Soc.* **2001**, *123*, 1215–1221. (c) Breitenbach, T.; Kuimova, M. K.; Gbur, P.; Hatz, S.; Schack, N. B.; Pedersen, B. W.; Lambert, J. D. C.; Poulsen, L.; Ogilby, P. R. *Photochem. Photobiol. Sci.* **2009**, *8*, 442–452.

(10) Abbotto, A.; Beverina, L.; Bozio, R.; Bradamante, S.; Ferrante, C.; Pagani, G. A.; Signorini, R. *Adv. Mater.* **2000**, *12*, 1963–1967.

(11) (a) Marder, S. R.; Perry, J. W.; Bourhill, G.; Gorman, C. B.; Tiemann, B. G.; Mansour, K. *Science* **1993**, *261*, 186. (b) Wortmann, R.; Poga, C.; Twieg, R. J.; Geletneky, C. *J. Chem. Phys.* **1996**, *105*, 10637–10647.

(12) (a) Zojer, E.; Beljonne, D.; Pacher, P.; Bredas, J.-L. *Chem.—Eur. J.* **2004**, *10*, 2668–2680. (b) Zojer, E.; Beljonne, D.; Kogej, T.; Vogel, H.; Marder, S. R.; Perry, J. W.; Brédas, J. L. *J. Chem. Phys.* **2002**, *116*, 3646–3658. (c) Barzoukas, M.; Blanchard-Desce, M. *J. Chem. Phys.* **2000**, *113*, 3951–3959. (d) Rumi, M.; Ehrlich, J. E.; Heikal, A. A.; Perry, J. W.; Barlow, S.; Hu, Z. Y.; McCord-Maughon, D.; Parker, T. C.; Rockel, H.; Thayumanavan, S.; Marder, S. R.; Beljonne, D.; Bredas, J. L. *J. Am. Chem. Soc.* **2000**, *122*, 9500–9510. (e) Beljonne, D.; Wenseleers, W.; Zojer, E.; Shuai, Z.; Vogel, H.; Pond, S. J. K; Perry, J. W.; Marder, S. R.; Brédas, J.-L. *Adv. Funct. Mater.* **2002**, *12*, 631–641.

(13) *Characterization Techniques and Tabulations for Organic Nonlinear Optical Materials*; Kuzyk, M. G., Dirk, C. W., Eds.; Marcel Dekker: New York, 1998.

(14) (a) Beverina, L.; Fu, J.; Leclercq, A.; Zojer, E.; Pacher, P.; Barlow, S.; Van Stryland, E. W.; Hagan, D. J.; Brédas, J.-L.; Marder, S. R. *J. Am. Chem. Soc.* **2005**, *127*, 7282–7283. (b) Kannan, R.; He, G. S.; Yuan, L. X.; Xu, F. M.; Prasad, P. N.; Dombroskie, A. G.; Reinhardt, B. A.; Baur, J. W.; Vaia, R. A.; Tan, L. S. *Chem. Mater.* **2001**, *13*, 1896–1904. (c) Belfield, K. D.; Schafer, K. J.; Mourad, W.; Reinhardt, B. A. *J. Org. Chem.* **2000**, *65*, 4475–4481. (d) Reinhardt, B. A.; Brott, L. L.; Clarson, S. J.; Dillard, A. G.; Bhatt, J. C.; Kannan, R.; Yuan, L. X.; He, G. S.; Prasad, P. N. *Chem. Mater.* **1998**, *10*, 1863–1874.

(15) Albota, M.; Beljonne, D.; Bredas, J. L.; Ehrlich, J. E.; Fu, J. Y.; Heikal, A. A.; Hess, S. E.; Kogej, T.; Levin, M. D.; Marder, S. R.; Mccordmaughon, D.; Perry, J. W.; Rockel, H.; Rumi, M.; Subramaniam, C.; Webb, W. W.; Wu, I. L.; Xu, C. *Science* **1998**, *281*, 1653–1656.

(16) Selected examples:(a) Chung, S.-J.; Zheng, S.; Odani, T.; Beverina, L.; Fu, J.; Padilha, L. A.; Biesso, A.; Hales, J. M.; Zhan, X.; Schmidt, K.; Ye, A.; Zojer, E.; Barlow, S.; Hagan, D. J.; VanStryland, E. W.; Yi, Y.; Shuai, Z.; Pagani, G. A.; Bredas, J. L.; Perry, J. W.; Marder, S. R. *J. Am. Chem. Soc.* **2006**, *128*, 14444–14445. (b) Kato, S.-I.; Matsumoto, T.; Shigeiwa, M.; Gorohmaru, H.; Maeda, S.; Ishi-i, T.; Mataka, S. *Chem.—Eur. J.* **2006**, *12*, 2303–2317. (c) Chung, S.-J.; Rumi, M.; Alain, V.; Barlow, S.; Perry, J. W.; Marder, S. R. *J. Am. Chem. Soc.* **2005**, *127*, 10844–10845. (d) Parent, M.; Mongin, O.; Kamada, K.; Katan, C.; Blanchard-Desce, M. *Chem. Commun.* **2005**, *15*, 2029–2031. (e) Woo, H. Y.; Liu, B.; Kohler, B.; Korystov, D.; Mikhailovsky, A.; Bazan, G. C. *J. Am. Chem. Soc.* **2005**, *127*, 14721–14729. (f) Halik, M.; Wenseleers, W.; Grasso, C.; Stellacci, F.; Zojer, E.; Barlow, S.; Bredas, J.-L.; Perry, J. W.; Marder, S. R. *Chem. Commun.* **2003**, *13*, 1490–1491. (g) Mongin, O.; Porres, L.; Moreaux, L.; Mertz, J.; Blanchard-Desce, M. *Org. Lett.* **2002**, *4*, 719–722. (h) He, G. S.; Lin, T.-C.; Prasad, P. N.; Kannan, R.; Vaia, R. A.; Tan, L.-S. *J. Phys. Chem. B* **2002**, *106*, 11081–11084. (i) Kim, O. K.; Lee, K. S.; Woo, H. Y.; Kim, K. S.; He, G. S.; Swiatkiewicz, J.; Prasad, P. N. *Chem. Mater.* **2000**, *12*, 284–286. (j) Ventelon, L.; Moreaux, L.; Mertz, J.; Blanchard-Desce, M. *J. Chem. Soc., Chem. Commun.* **1999**, *20*, 2055–2056. (k) Belfield, K. D.; Hagan, D. J.; Van Stryland, E. W.; Schafer, K. J.; Negres, R. A. *Org. Lett.* **1999**, *1*, 1575–1578.

(17) (a) Abbotto, A.; Beverina, L.; Manfredi, N.; Pagani, G. A.; Archetti, G.; Kuball, H.-G.; Wittenburg, C.; Heck, J.; Holtmann, J. *Chem.—Eur. J.* **2009**, *15*, 6175–6185. (b) Archetti, G.; Abbotto, A.; Wortmann, R. *Chem.—Eur. J.* **2006**, *12*, 7151–7160. (c) Abbotto, A.; Beverina, L.; Bradamante, S.; Facchetti, A.; Klein, C.; Pagani, G. A.; Redi-Abshiro, M.; Wortmann, R. *Chem.—Eur. J.* **2003**, *9*, 1991–2007. (d) Abbotto, A.; Bradamante, S.; Pagani, G. A. *J. Org. Chem.* **2001**, *66*, 8883–8892. (e) Abbotto, A.; Bradamante, S.; Facchetti, A.; Pagani, G. A. *J. Org. Chem.* **1997**, *62*, 5755–5765.

(18) (a) Abbotto, A.; Beverina, L.; Bozio, R.; Facchetti, A.; Ferrante, C.; Pagani, G. A.; Pedron, D.; Signorini, R. *Org. Lett.* **2002**, *4*, 1495–1498. (b) Abbotto, A.; Beverina, L.; Bozio, R.; Bradamante, S.; Facchetti, A.; Ferrante, C.; Pagani, G. A.; Pedron, D.; Signorini, R. *NATO Sci. Ser. II* **2003**, *100*, 385–393. (c) Signorini, R.; Ferrante, C.; Pedron, D.; Zerbetto, M.; Cecchetto, E.; Slaviero, M.; Fortunati, I.; Collini, E.; Bozio, R.; Abbotto, A.; Beverina, L.; Pagani, G. A. *J. Phys. Chem. A* **2008**, *112*, 4224–4234.

(19) Abbotto, A.; Beverina, L.; Bozio, R.; Facchetti, A.; Ferrante, C.; Pagani, G. A.; Pedron, D.; Signorini, R. *Chem. Commun.* **2003**, *17*, 2144–2145.

(20) Katritzky, A. R. *Handbook of Heterocyclic Chemistry*; Pergamon Press: Oxford, U.K., 1983. Bradamante, S.; Pagani, G. In *Advances in Carbanion Chemistry*; Snieckus, V., Ed.; JAI Press: Greenwich CT, 1996; Vol. 2, pp 189−263.

(21) (a) Abbotto, A.; Bradamante, S.; Facchetti, A.; Pagani, G. A. *J. Org. Chem.* **1999**, *64*, 6756–6763. (b) Abbotto, A.; Bradamante, S.; Facchetti, A.; Pagani, G. A. *J. Org. Chem.* **1998**, *63*, 436–444. (c) Abbotto, A.; Bradamante, S.; Pagani, G. A.; Rzepa, H.; Stoppa, F. *Heterocycles* **1995**, *40*, 757–776. (d) Abbotto, A.; Alanzo, V.; Bradamante, S.; Pagani, G. A. *J. Chem. Soc., Perkin Trans. 2* **1991**, 481–488. (e) Bradamante, S.; Pagani, G. A. *Pure Appl. Chem.* **1989**, *61*, 709–716. (f) Raposo, M. M. M.; Sousa, A. M. R. C.; Kirsch, G.; Cardoso, P.; Belsley, M.; De Matos Gomes, E.; Fonseca, A. M. C. *Org. Lett.* **2006**, *8*, 3681–3684.

(22) (a) Abbotto, A.; Baldini, G.; Beverina, L.; Chirico, G.; Collini, M.; D'Alfonso, L.; Diaspro, A.; Magrassi, R.; Nardo, L.; Pagani, G. A. *Biophys. Chem.* **2005**, *114*, 35–41. (b) Versari, S.; Villa, A. M.; Villa, A.; Doglia, S. M.; Pagani, G. A.; Bradamante, S. *J. Biomed. Opt.* **2006**, *11*, 034014−4.

(23) Reichardt, C. *Chem. Rev.* **1994**, *94*, 2319–2358.

(24) (a) Kanis, D. R.; Ratner, M. A.; Marks, T. J. *Chem. Rev.* **1994**, *94*, 195–242. Bredas, J. L.; Cornil, K.; Meyers, F.; Beljonne, D., in: SkotheimT. A. Elsenbaumer, R. L., Reynolds, J. R. *Handbook of Conducting Polymers*; Marcel Dekker: New York, 1998; p. 1. (b) Bishop, D. M. *Int. Rev. Phys. Chem.* **1994**, *13*, 21–39, and references therein.

(25) (a) Painelli, A. *Chem. Phys.* **1999**, *245*, 185–197. (b) Painelli, A.; Terenziani, F. *Chem. Phys. Lett.* **1999**, *312*, 211–220. (c) Painelli, A.; Terenziani, F. *J. Phys. Chem. A* **2000**, *104*, 11041–11048. (d) Terenziani, F.; Painelli, A.; Comoretto, D. *J. Phys. Chem. A* **2000**, *104*, 11049–11054. (e) Boldrini, B.; Cavalli, E.; Painelli, A.; Terenziani, F. *J. Phys. Chem. A* **2002**, *106*, 6286–6294. (f) Terenziani, F.; Painelli, A.; Girlando, A.; Metzger, R. M. *J. Phys.Chem. B* **2004**, *108*, 10743–10750.

(26) Terenziani, F.; Painelli, A.; Katan, C.; Charlot, M.; Blanchard-Desce, M. *J. Am. Chem. Soc.* **2006**, *128*, 15742–15755.

(27) (a) Terenziani, F.; Sissa, C.; Painelli, A. *J. Phys. Chem. B* **2008**, *112*, 5079–5087. (b) Sissa, C.; Terenziani, F.; Painelli, A. *J. Phys. Chem. A* **2008**, *112*, 8697–8705.

(28) (a) Painelli, A.; Terenziani, F. In *Non-linear optical properties of matter: From molecule to condensed phases*; Papadopoulos, M. G., Leszczynski, J., Sadlej, J., Eds.; Springer: Dordrecht, The Netherlands, 2006; pp 251−282. (b) Painelli, A.; Terenziani, F.; Soos, Z. G. *Theor. Chem. Acc.* **2007**, *117*, 915–931. (c) Terenziani, F.; D'Avino, G.; Painelli, A. *ChemPhysChem* **2007**, *8*, 2433–2444.

(29) (a) Painelli, A.; Terenziani, F. *J. Am. Chem. Soc.* **2003**, *125*, 5624–5625. (b) Terenziani, F.; Painelli, A. *Phys. Rev. B* **2003**, *68*, 155405.

(30) D'Avino, G.; Terenziani, F.; Painelli, A. *J. Phys. Chem. B* **2006**, *110*, 25590–25592.

(31) (a) D'Avino, G.; Grisanti, L.; Guasch, J.; Ratera, I.; Veciana, J.; Painelli, A. *J. Am. Chem. Soc.* **2008**, *130*, 12064–12072. (b) D'Avino, G.; Grisanti, L.; Painelli, A.; Guasch, J.; Ratera, I.; Veciana, J. *Cryst. Eng. Commun.* **2009**, *11*, 2040–2046.

(32) Girlando, A.; Sissa, C.; Terenziani, F.; Painelli, A.; Chwialkowska, A.; Ashwell, G. J. *ChemPhysChem.* **2007**, *8*, 2195.

(33) (a) Terenziani, F.; Angiolini, L.; Benelli, T.; Giorgini, L. *Chem.—Eur. J.* **2005**, *11*, 6053–6063. (b) Datta, A.; Terenziani, F.; Painelli, A. *ChemPhysChem* **2006**, *7*, 2168–2174. (c) Liang, K.; Farahat, M. S.; Perlstein, J.; Law, K.-Y.; Whitten, D. G. *J. Am. Chem. Soc.* **1997**, *119*, 830–831. (d) Ajayaghosh, A.; Arunkumar, E.; Daub, J. *Angew. Chem., Int. Ed.* **2002**, *41*, 1766–1769. (e) Arunkumar, E.; Chithra, P.; Ajayaghosh, A. *J. Am. Chem. Soc.* **2004**, *126*, 6590–6598. (f) Arunkumar, E.; Ajayaghosh, A.; Daub, J. *J. Am. Chem. Soc.* **2005**, *127*, 3156–3164. (g) Liao, Y.; Bhattacharjee, S.; Firestone, K. A.; Eichinger, B. E.; Paranji, R.; Anderson, C. A.; Robinson, B. H.; Reid, P. J.; Dalton, L. R. *J. Am. Chem. Soc.* **2006**, *128*, 6847–6853. (h) Liao, Y.; Firestone, K. A.; Bhattacharjee, S.; Luo, J.; Haller, M.; Hau, S.; Anderson, C. A.; Lao, D.; Eichinger, B. E.; Robinson, B. H.; Reid, P. J.; Jen, A. K.-Y.; Dalton, L. R. *J. Phys. Chem. B* **2006**, *110*, 5434–5438. (i) Hennrich, G.; Murillo, M. T.; Prados, P.; Song, K.; Asselberghs, I.; Clays, K.; Persoons, A.; Benet-Buchholz, J.; de Mendoza, J. *Chem. Commun.* **2005**, *21*, 2747–2749.

(34) (a) Terenziani, F.; Morone, M.; Gmouh, S.; Blanchard-Desce, M. *ChemPhysChem* **2006**, *7*, 685–696. (b) Terenziani, F.; Ghosh, S.; Robin, A.-C.; Das, P. K.; Blanchard-Desce, M. *J. Phys. Chem. B* **2008**, *112*, 11498–11505. (c) Terenziani, F.; Mongin, O.; Katan, V; Bhatthula, B. K. G.; Blanchard-Desce, M. *Chem.—Eur. J.* **2006**, *12*, 3089–3102.

(35) (a) Abbotto, A.; Beverina, L.; Pagani, G. A.; Collini, M.; Chirico, G.; D'Alfonso, L.; Baldini, G. *SPIE Proc.* **2003**, *5139*, 223–230. (b) Facchetti, A.; Beverina, L.; Van der Boom, M., E.; Dutta, P.; Evmenenko, G.; Shukla, A. D.; Stern, C. E.; Pagani, G. A.; Marks, T. J *J. Am. Chem. Soc.* **2006**, *128*, 2142–2153.

(36) Salomon, M. F.; Salomon, R. G. *J. Am. Chem. Soc.* **1979**, *101*, 4290–4299.

(37) Gutman, V. *The Donor-Acceptor Approach to Molecular Interactions*; Plenum Press: New York, 1978; Chapters 7 and 10.

(38) (a) Craig, D. P.; Walmsley, S. H. *Excitons in Molecular Crystals*; Benjamin: New York 1968. (b) Davydov, A. S. *Theory of Molecular Excitons*; Plenum Press: New York, 1971. (c) Craig, D. P. *J. Chem. Soc.* **1955**, 2302–2308. (d) Pope, M.; Swenberg, C. E. *Electronic Processes in Organic Crystals and Polymers*; Oxford Univeristy Press: New York, 1999. (e) Silinsh, E. A.; Capek, V. *Organic Molecular Crystals*; AIP Press: New York, 1994. (f) Knoester, J. In *Organic Nanostructures: Science and Applications*; Proceedings of the International School of Physics Enrico Fermi, CXLIX Course; Agranovich, M., La Rocca, G. C., Eds.; IOS Press: Amsterdam, 2002.

(39) Mulliken, R. S. *J. Am. Chem. Soc.* **1952**, *74*, 811–824.

JP909475D